

# Chapter 7

## E1111: Subsidiary $\mu^+$ SR experiment

### 7.1 Introduction

In December 2006, members of TWIST and CMMS<sup>42</sup> recorded two weeks of muon spin relaxation ( $\mu^+$ SR) data using high purity metal stopping targets. The arrival time of decay positrons were recorded (“time differential  $\mu$ SR”). The M20 beam line was used with  $\mu$ SR “Knight shift” apparatus. The acceptance of the detector was determined using a calibration sample of the spin glass  $\text{Gd}_2\text{Ti}_2\text{O}_7$ , and measurements of depolarisation were made for aluminium and silver targets constructed from the same foils as the main experiment. The samples were immersed in a 2.0 T longitudinal magnetic field, and the temperature and pressure were the same as the room’s surroundings; these conditions match the TWIST detector. This chapter will briefly describe the experiment and how the results impact the main experiment. Note this is one of the highest precision experiments ever carried out using  $\mu^+$ SR apparatus.

There were two experimental aims. Firstly,  $\mu^+$ SR can measure asymmetry down to a time scale of about 5 ns since it uses fast scintillators to count decay positrons. In contrast, TWIST’s minimum decay time is nominally 1  $\mu\text{s}$ , due to a possible upstream inefficiency from muon ionisation overlapping decay position ionisation in the slow drift chambers. For the asymmetry measurements in this thesis, the lower time limit was pushed to 0.46  $\mu\text{s}$ , which still allows for an undetected fast depolarisation component. A lack of additional depolarisation components down to 5 ns would improve confidence in the main experiment’s results. At the time of writing, this is probably the shortest time scale that can be experimentally observed, and there are few credible models for a depolarisation below 5 ns in metals. Secondly, the rate is much higher in  $\mu^+$ SR (20 – 40 kHz compared to 2 – 5 kHz), which should have allowed a high statistics measurement of the depolarisation rate comparable to the main experiment. However, this second goal was not achieved due to the length of time required to calibrate the apparatus, and the dominant systematic uncertainty due to the fraction of muons stopping in the trigger scintillator, which will be described in detail later in this chapter.

---

<sup>42</sup>TRIUMF Centre for Molecular & Materials Science.

## 7.2 Theory

Recall the differential decay probability for obtaining an  $e^+$  from  $\mu^+$  decay,

$$\frac{d^2\Gamma}{dx d\cos\theta} = \frac{G_F^2 m_\mu^5}{192\pi^3} [3 - 2x + P_\mu \cos\theta(2x - 1)] x^2, \quad (7.1)$$

where  $\theta$  is the angle between the electron momentum and muon spin,  $P_\mu$  is the degree of muon polarisation, and  $x \equiv 2E_e/m_\mu$ . This equation assumes standard model couplings, and ignores radiative corrections, neutrino masses and positron mass. If decay positrons are detected for energy  $p < x < q$  with 100% efficiency then

$$\begin{aligned} \frac{d\Gamma}{d\cos\theta} = \int_p^q dx \frac{d^2\Gamma}{dx d\cos\theta} &= \frac{G_F^2 m_\mu^5}{192\pi^3} \left\{ \left[ (q^3 - p^3) - \frac{1}{2}(q^4 - p^4) \right] \right. \\ &\quad \left. + P_\mu \cos\theta \left[ \frac{1}{2}(q^4 - p^4) - \frac{1}{3}(q^3 - p^3) \right] \right\}, \end{aligned} \quad (7.2)$$

and if the angular fiducial is  $a < \cos\theta < b$  then the normalised number of counts is given by

$$N = \frac{G_F^2 m_\mu^5}{192\pi^3} (b - a) \left[ (q^3 - p^3) - \frac{1}{2}(q^4 - p^4) \right] (1 + AP_\mu), \quad (7.3)$$

$$A = \frac{1}{2}(b + a) \frac{\frac{1}{2}(q^4 - p^4) - \frac{1}{3}(q^3 - p^3)}{(q^3 - p^3) - \frac{1}{2}(q^4 - p^4)}. \quad (7.4)$$

Even under the assumption of 100% efficiency, the decay rate is already a complicated function of reduced energy and angle. Assuming there are counters in the forward ( $-1 < \cos\theta < 0$ ) and backward ( $0 < \cos\theta < 1$ ) directions, and each of these counters have their own values of  $\{a, b, p, q\}$  and an associated background, Eq. (7.3) can be used to show

$$n_b(t) = b_b + N_0 e^{-t/\tau_\mu} [1 + A_b P_\mu(t)] \quad (7.5)$$

$$n_f(t) = b_f + r N_0 e^{-t/\tau_\mu} [1 - A_f P_\mu(t)]. \quad (7.6)$$

where  $n_b$  and  $n_f$  are the number of backward and forward counts,  $b_b$  and  $b_f$  are the backgrounds in each counter,  $\tau_\mu$  is the muon lifetime,  $N_0$  is the number of muons at  $t = 0$  multiplied by the factors in Eq. (7.3), and  $r$  accounts for differences in energy and angle acceptance between the counters.  $A_b$  and  $A_f$  are expected to only depend on the counter geometry and material that a positron passes through, and should remain the same if counters are not moved and the target material is unchanged. If  $P_\mu = P_\mu(0)f(t)$ , where  $f(t)$  is the time dependent part, then Eqs. (7.5) and (7.6) cannot separate  $P_\mu(0)$  from the  $A$ 's unless  $r$ ,  $A_b$  and  $A_f$  are determined by other means (e.g. by a Monte Carlo simulation). Therefore  $\mu^+$ SR cannot measure  $P_\mu(0)$  with high precision, and should only be used to determine  $f(t)$ , the time dependent part of the polarisation.

## 7.3 Apparatus

### 7.3.1 Sample preparation

Aluminium and silver samples from the same foil as the TWIST targets were stacked several layers thick<sup>43</sup>, and clamped together with x-ray Mylar. There was no grease or glue used. The multiple layers meant the muons had negligible probability of passing through the target.

A calibration sample was needed to determine  $A_b$  and  $A_f$  in Eqs. (7.5) and (7.6), which are the acceptances of the counters. The TRIUMF CMMS group recommended a spin glass,  $\text{Gd}_2\text{Ti}_2\text{O}_7$ , which from here on will simply be referred to as “spin glass”<sup>44</sup>. This was known to depolarise in several microseconds with an expected exponential form. The CMMS group provided a disc of approximately 3.0 cm diameter and mass 4.5 g.

### 7.3.2 M20 Beam line

Muons were delivered to the stopping target by the M20 beam line, which is a dedicated surface muon source also located at TRIUMF, in the same experimental hall as the main experiment's M13 beam line. The channel has been described elsewhere[52], and is similar to M13, with the addition of a spin rotator (DC separator) element, which selects particles by velocity to remove most positrons originating from the production target. This is important for  $\mu$ SR since there is no event information, and a scattered beam positron can trigger the

---

<sup>43</sup>The aluminium target was ten layers thick, and the silver had six layers.

<sup>44</sup>The spin glass is a geometrically frustrated anti-ferromagnet. The condensed matter community have studied the muon depolarisation within the material to determine the local magnetic fields [51], but have not undertaken precision tests. The important fact for TWIST is that the sample rapidly and completely depolarises muons that stop within it.

annular forward or backward counters in the same way as a decay positron. The DC separator has the disadvantage of introducing significant transverse polarisation components. M20 has a momentum acceptance that is larger than M13, and was not determined for this experiment. The beam spot is also larger than M13, meaning collimation is necessary, which will lead to a background from lower momentum slit-scattered particles.

### 7.3.3 Detector

The detector is shown schematically in Fig. 7.1, where muons can either stop in the high purity silver mask, the sample under investigation, or one of the trigger scintillators. This

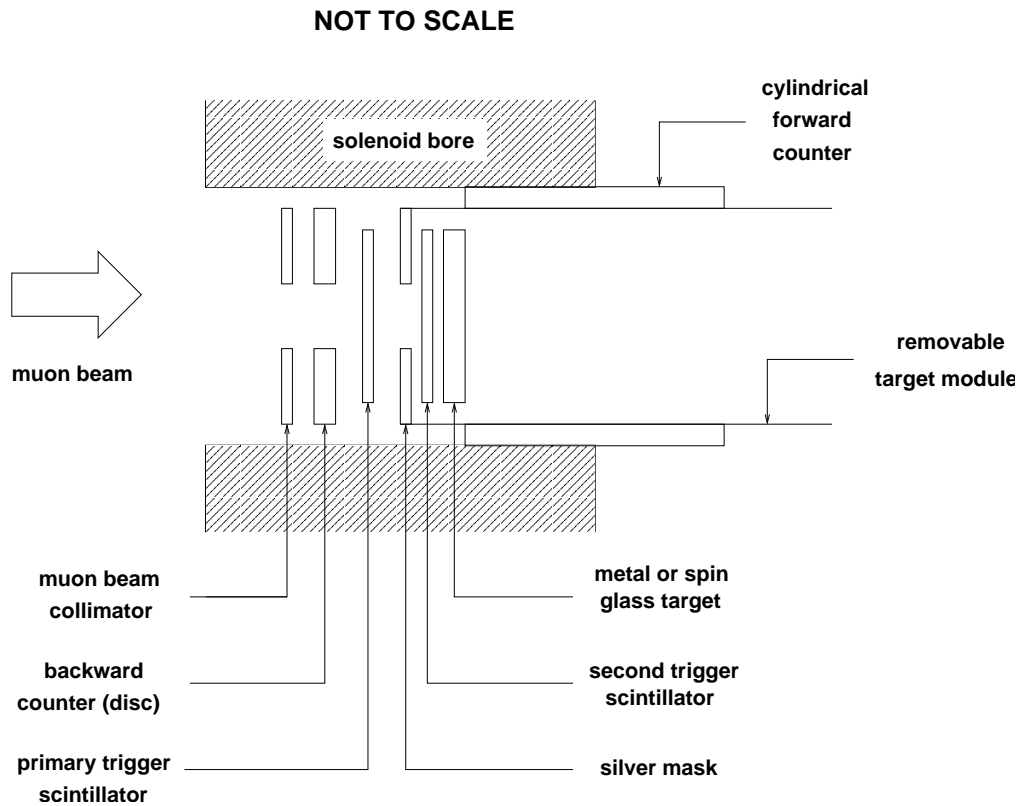


Figure 7.1: Schematic for the experimental setup. The muons enter from the left and will start an event if they pass through the first scintillator and decay in the silver mask, or pass through both scintillators and decay in the metal target. The figure shows the counters are annular, and not directly in the path of the beam. Note that not all materials are shown, such as vacuum tubes, light guides and the beam pipe.

arrangement allows the experiment to simultaneously measure the sample and the silver in the mask (the “reference silver”). The results for the silver mask are expected to remain

constant for the experiment and can be used to detect changes in the running conditions. Note the forward and backward counters are approximately 0.6 cm thick. The backward counter is a disc of approximately 8.0 cm diameter, with a 2.5 cm hole for the muon beam. The target module was placed in the  $\mu$ SR HELIOS superconducting solenoid [53].

The thresholds in the electronics are set to have a very high muon detection efficiency, rather than for total beam positron removal. Therefore the experiment has a background. Multiple muons are removed by the electronics, so the background is made up of cosmics, scattered positrons, and muon decays before the target. Decays in or near the collimator are expected to be the dominant source. The removal of multiple muons  $14 \mu\text{s}$  either side of the event ensures the background does not contain time dependent parts due to muon decay.  $\mu$ SR does not record event information, meaning the background in each counter must be either subtracted, or included in the fit. For this experiment, events for  $1 \mu\text{s}$  before the muon trigger were recorded for each event. The aim was to fix the background to these “ $t < 0$ ” values, which should be made up of random time-independent noise.

## 7.4 Data

The experiment collected data from 6 December 2006 to 20 December 2006, in runs that lasted between five and fourteen hours. The conditions of TWIST were matched; the sample was immersed in a longitudinal 2 T magnetic field, and the temperature was not controlled<sup>45</sup>. The experiment started by taking runs with a spin glass target. During these initial runs, the beam line was adjusted for rate and beam quality. A few days into the experiment, it was realised that the detector acceptance needed to be determined with a target of spin glass *and* metal, back-to-back. The target materials were then reversed to determine the metal depolarisation. This technique was supposed to keep the amount of material seen by the decay positrons constant. The report will later show that variations in  $r$  suggest this aim was not completely achieved.

The data has been divided into sets, which are summarised in chronological order in Table 7.1. There were unscheduled interruptions during data acquisition, and the runs immediately after these interruptions were low rate and have been rejected. The bad runs have already been removed from the totals in the table.

The limited geometry of the decay positron counters (see Fig. 7.1) results in a total positron rate approximately 10% lower than the muon rate. Approximately half of the beam

---

<sup>45</sup>Initially, there was a plan to test the validity of the Korringa relaxation model. This model predicts a relaxation rate,  $\lambda$ , which should be independent of magnetic field, but show an increase with temperature. However, due to the limited beam time this test was abandoned in favour of the primary TWIST aims.

time was spent on the nominal sets (E to H). The rate changed between the unscheduled interruptions, which are indicated by horizontal lines in the table. Set D was supposed to have only an exaggerated DC separator setting, but it is also low rate.

A surface muon edge scan was not carried out, so the exact beam line momentum and resolution are undetermined.

Table 7.1: The table shows the division of the data into sets, where a “set” is defined as a sum of individual runs. The horizontal lines indicate when data taking was suspended.

Data set	Target	Description	Duration (hours)	$\mu^+$ rate		$\mu^+$ counts	
				reference (kHz)	sample (kHz)	reference ( $\times 10^9$ )	sample ( $\times 10^9$ )
A	SG <sup>a</sup>	calibration	14.1	24.4	15.2	1.2	0.8
B	Al	nominal Al	8.0	25.0	15.6	0.7	0.5
C	Al	$\frac{1}{2}$ -rate	15.7	12.4	9.6	0.7	0.5
D	Al	DC sep. high	5.7	16.6	10.7	0.3	0.2
E	SG+Al	nominal SG	24.0	19.4	13.3	1.7	1.2
F	Al+SG	nominal Al	40.1	19.9	13.7	2.9	2.0
G	Ag+SG	nominal Ag	32.4	21.8	14.6	2.5	1.7
H	SG+Ag	nominal SG	22.8	21.6	14.5	1.8	1.2
I	SG+Ag	thick scint. <sup>b</sup>	18.0	20.7	14.0	1.3	0.9
J	SG+Ag	thin scint. <sup>c</sup>	22.2	18.3	12.5	1.5	1.0
K	Ag+SG	thin scint.	13.3	20.1	13.8	1.0	0.7

<sup>a</sup> SG = Spin Glass.

<sup>b</sup> The thick scintillator was  $508 \mu\text{m}$ , which is double the nominal thickness.

<sup>c</sup> The thin scintillator was  $127 \mu\text{m}$ , which is half the nominal thickness.

## 7.5 Analysis

Figure 7.1 described the geometry of four positron counters (two for the sample, and two for the reference silver). The data acquisition system (DAQ) recorded the positron time of arrival in each of these counters, using 19200 channels of width  $0.78125 \text{ ns}$ . Data were recorded  $1 \mu\text{s}$  before the muon trigger, and  $14 \mu\text{s}$  afterwards. The DAQ software determined  $t = 0$ , and inspection of the four histograms suggested that good data started 8 bins ( $10 \text{ ns}$ ) away from the  $t = 0$  bin.

The aim of the analysis was to simultaneously fit Eq. (7.5) to the backward counts and

Eq. (7.6) to the forward counts<sup>46</sup>. The spin glass calibration sample would be fit with  $P_\mu(t) = \exp(-\lambda t)$ , which determines  $A_b$  and  $A_f$ . These parameters would then be fixed while fitting the metal samples.

### 7.5.1 Rebinning

The fit functions assumed a background that has no time dependence, and a muon beam with no transverse polarisation. In reality, protons arrive at the muon production target in bunches separated by the cyclotron period (43 ns), causing a time dependence to the background. In addition, the transverse polarisation component precesses at the Larmor frequency ( $\omega = g_\mu B = 272$  MHz). Since these effects are not included in the fit functions, the histograms of counts must be carefully rebinned to minimise their effect.

The DAQ software performed a Fourier transform, and found peaks at 23.06 MHz (43.37 ns) and 271.67 MHz (3.68 ns). This suggested the rebinnings in Table 7.2. A robustness test was carried out by fitting a spin glass run with between 10 and 500 channels combined. The  $\chi^2/\text{ndof}$  and  $A_b$  are shown in Fig. 7.2. The final choice combined 115 bins (89.84 ns), which avoids both the gaps in the figure that correspond to failed fits, and the region for less than 60 combined channels where the reduced  $\chi^2$  starts to show a systematic increase. The  $A_b$  parameter in Fig. 7.2(b) is reassuringly robust to the choice. The other fit parameters are similarly robust, but are not shown here. The discrepancy between the options in Table 7.2 and Fig. 7.2 probably arise from the Fourier transform being carried out on a simple forward-backward asymmetry<sup>47</sup>, which has distortions since it assumes identical forward and backward counter acceptances.

---

<sup>46</sup>Alternative parametrisations were tried, such as multiplying  $b_f$  by  $r$ ,

$$n_f(t) = rb_f + rN_0e^{-t/\tau_\mu} [1 + A_fP_\mu(t)], \quad (7.7)$$

and making  $N_0$  an overall factor,

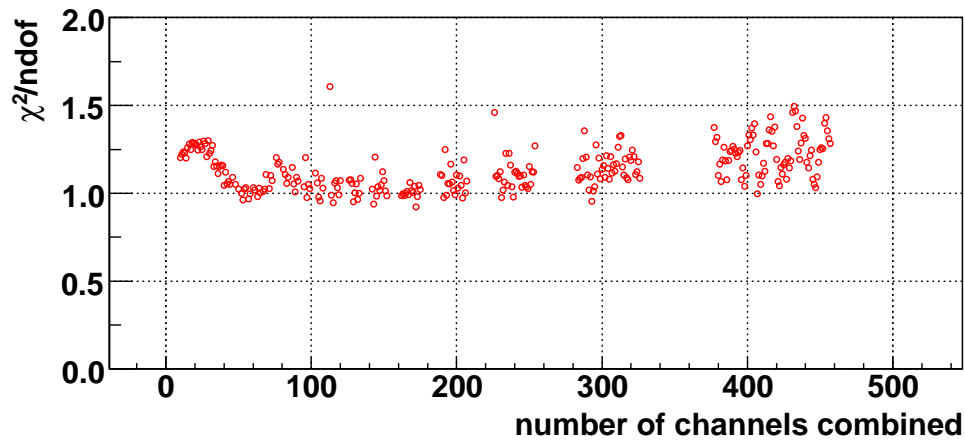
$$n_f(t) = N_0 \left\{ b_f + re^{-t/\tau_\mu} [1 + A_fP_\mu(t)] \right\}. \quad (7.8)$$

However, neither of these offered any advantage.

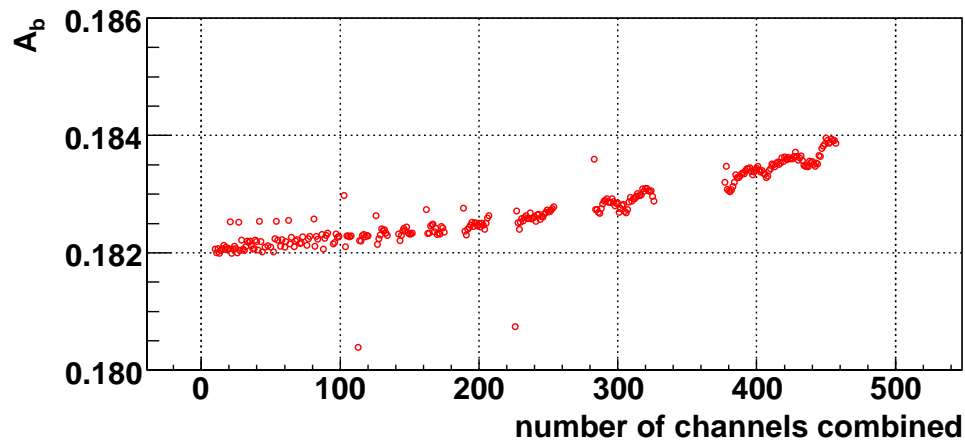
<sup>47</sup>In other words, the asymmetry was constructed from  $(N_B - N_F)/(N_B + N_F)$ , where  $N_B$  and  $N_F$  are the number of counts in the backward and forward counters.

Table 7.2: The raw data has 19200 channels with spacing 0.78125 ns. The cyclotron period is 43.37 ns, and the Larmor precession period is 3.68 ns. The channels must be combined to “bin-out” these periods.

number of channels to combine	cyclotron periods	precession periods
113	2.04	23.99
165	2.97	35.03
278	5.01	59.02
391	7.04	83.01
443	7.98	94.05



(a) Rebinning effect on reduced  $\chi^2$ .



(b) Backward counter acceptance parameter,  $A_b$ .

Figure 7.2: Results of fitting a single spin glass calibration run with between 10 and 500 channels combined.

## 7.5.2 Calibration using spin glass

Table 7.1 shows there are five data sets where the target material was spin glass (SG). These were fit assuming an exponential depolarisation,  $P_\mu(t) = P_\mu(0) \exp(\lambda_{\text{SG}}t)$ . The individual runs within a set were checked for consistency, and the results for each set are compared in Fig. 7.3. The numerical results are included as Table 7.3.

The results for the double-thickness scintillator are anomalous. In this case, a significant fraction of muons must be stopping and depolarising in the scintillator, and a single exponential model is inappropriate. The fit's confidence level is lower (14%), but not unreasonable, which indicates the data has poor sensitivity to an extra depolarisation term for the scintillator. The results for the thin scintillator are consistent with the nominal case, suggesting the fraction of muons stopping in the nominal scintillator must be small.

The  $A_b$  and  $A_f$  parameters depend on the target, which confirms the importance of calibrating with a target of spin glass backed with metal, rather than spin glass alone. The  $r$  parameters vary by significant amounts between sets, but are consistent between the runs within sets. This suggests the parameter is extremely sensitive to the geometry (e.g. target

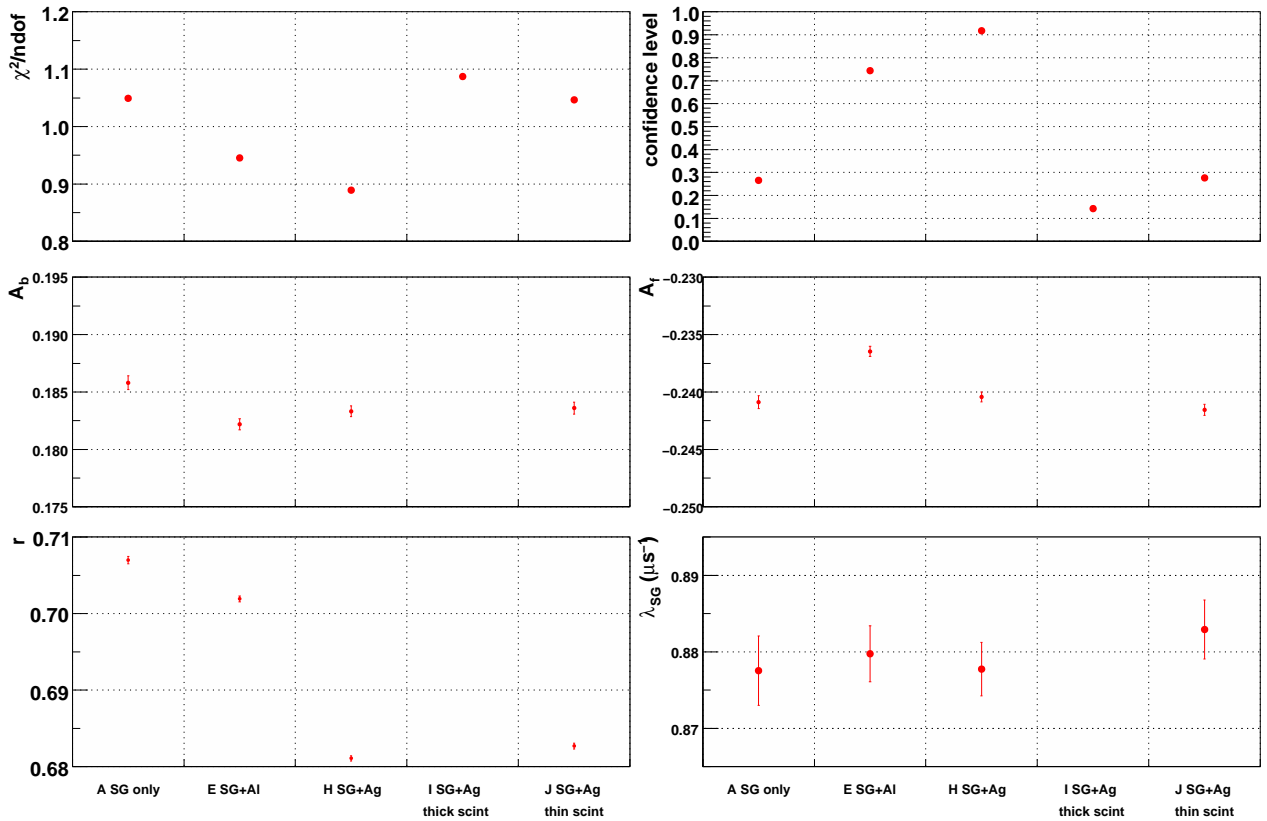


Figure 7.3: Fit parameters for the spin glass (SG) calibration sample.

placement); this has been observed by previous  $\mu^+$ SR experimenters[54]. The  $r$  parameter must be left free when the metal samples are fit.

The backgrounds in each counter were investigated. When the backgrounds were free fit parameters, the values had a significant statistical discrepancy ( $> 3\sigma$ ) from the result using the  $1\ \mu\text{s}$  of  $t < 0$  counts. Since the backgrounds could be determined using the  $t > 0$  decay data, and had a weak correlation with the other fit parameters, the  $t < 0$  data were rejected.

Table 7.3: Fit parameters for a single exponential fit to the spin glass sets. The bracketed number indicates the statistical uncertainty on the final digit.

Set	A	E	H	I	J
Sample	SG	SG+Al	SG+Ag	SG+Ag	SG+Ag
Scintillator thickness ( $\mu\text{m}$ )	254	254	254	508	127
$\chi^2/\text{ndof}$	316.9/302 = 1.05	285.5/302 = 0.95	268.5/302 = 0.89	328.3/302 = 1.09	316.1/302 = 1.05
Confidence	0.27	0.74	0.92	0.14	0.28
$r$	0.7070 (5)	0.7019 (4)	0.6811 (3)	0.4764 (5)	0.6827 (4)
$A_b$	0.1858 (6)	0.1822 (5)	0.1833 (5)	0.0276 (5)	0.1836 (5)
$A_f$	-0.2409 (6)	-0.2365 (4)	-0.2404 (4)	-0.0522 (7)	-0.2415 (5)
$\lambda_{\text{SG}}(\mu\text{s}^{-1})$	0.878 (5)	0.880 (4)	0.878 (4)	0.553 (18)	0.883 (4)

Alternative models for  $P_\mu(t)$  in the spin glass were tried, even though the reduced  $\chi^2$  values suggested there would be minimal sensitivity. A variable power law,  $P_\mu(t) = \exp(-at^p)$ , found  $p = (1.005 \pm 0.007)$  for set E (SG+Al), with no change in the reduced  $\chi^2$ . A sum of single exponentials was also tried, but the minimisation using MINUIT was unsuccessful for the nominal spin glass sets.

A substantial effort was made to determine the depolarisation within the trigger scintillator, using the set taken with the double thickness ( $508\ \mu\text{m}$ ) scintillator where a significant fraction of muons stopped in the trigger. The first approach was iterative:

1. Fit  $127\ \mu\text{m}$  set assuming 100% muons stop in the sample, to determine  $\lambda_{\text{SG}}$ .
2. Fit  $508\ \mu\text{m}$  set allowing for stops in both the scintillator and sample using

$$P_\mu(t) = \epsilon \exp(-\lambda_{\text{scint}}t) + (1 - \epsilon) \exp(-\lambda_{\text{SG}}t), \quad (7.9)$$

where  $\epsilon$  is the fraction of muons stopping in the trigger scintillator,  $\lambda_{\text{scint}}$  is the relaxation rate in the scintillator, and  $\lambda_{\text{SG}}$  was fixed to the  $127\ \mu\text{m}$  value from (1).

3. Fit 127  $\mu\text{m}$  set with Eq. (7.9), with  $\epsilon$  and  $\lambda_{\text{scint}}$  fixed to the values from (2).
4. Iterate (2)-(3) until convergence.

Only two iterations were required, and the results for the 127  $\mu\text{m}$  and 508  $\mu\text{m}$  sets are shown in Table 7.4. There is a reduction in  $\chi^2$  when including a second exponential, and the high confidence level suggests that a single exponential model is valid for depolarisation in the scintillator. The  $r$ ,  $A_b$  and  $A_f$  parameters become more consistent with the other spin glass fits. For the thin scintillator, the  $\chi^2$  is changed minimally, and the fraction of muons stopping in the scintillator is consistent with zero. The uncertainties for the 127  $\mu\text{m}$  scintillator fit

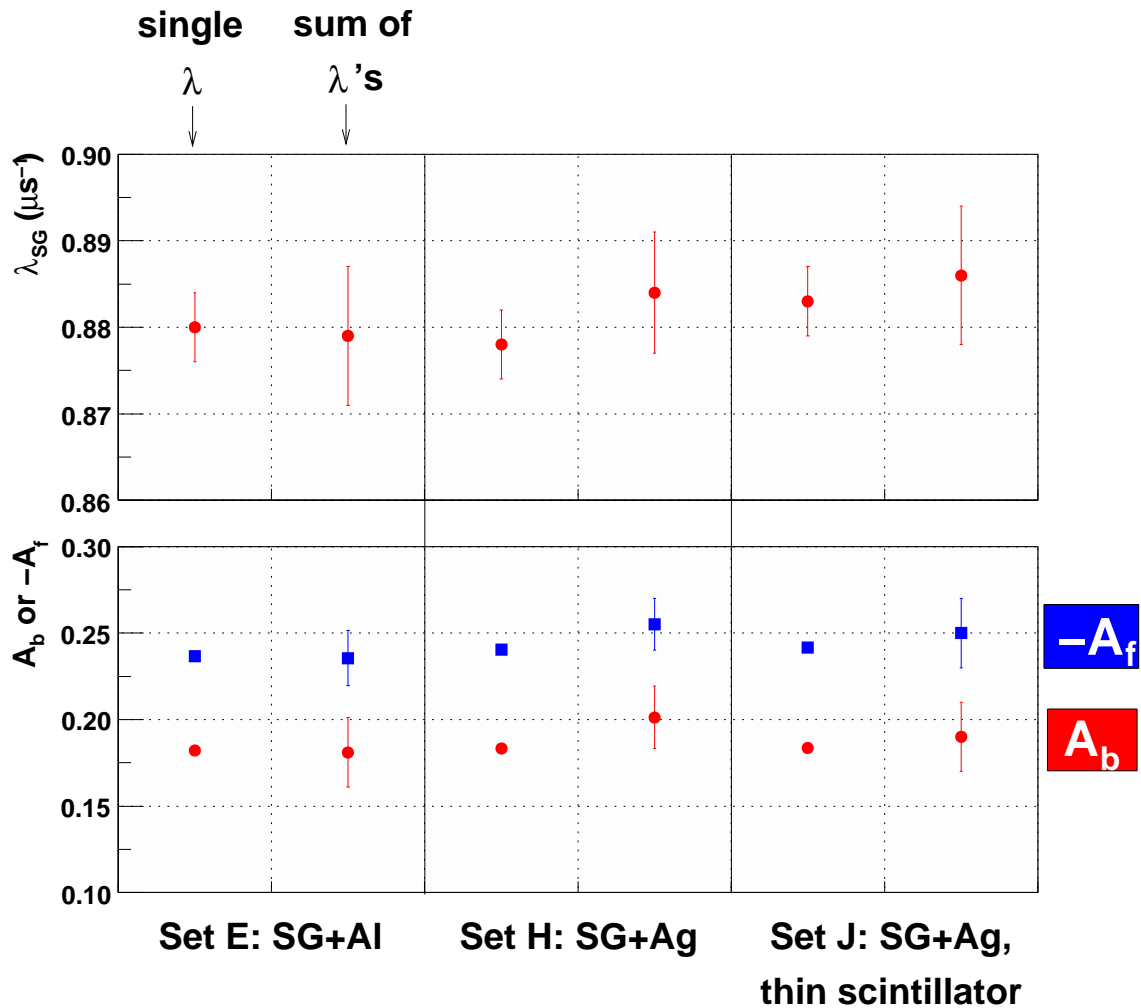
Table 7.4: Comparison of fit parameters for single exponential and sum of exponentials, where the latter allows for separate depolarisation in the spin glass and scintillator. The bracketed number indicates the statistical uncertainty on the final digit.

Set	Set I: SG+Ag, 508 $\mu\text{m}$ scint.		Set J: SG+Ag, 127 $\mu\text{m}$ scint.	
Fit	Single $\lambda$	Converged	Single $\lambda$	Converged
$\chi^2/\text{ndof}$	328.3/302	284.5/301	316.1/302	315.9/301
	= 1.09	= 0.95	= 1.05	= 1.05
Confidence	0.14	0.74	0.28	0.27
$r$	0.4764 (5)	0.648 (1)	0.6827 (4)	0.69 (3)
$A_b$	0.0276 (5)	0.157 (1)	0.1836 (5)	0.19 (2)
$A_f$	-0.0522 (7)	-0.218 (2)	-0.2415 (5)	-0.25 (2)
$\lambda_{\text{SG}} (\mu\text{s}^{-1})$	0.553 (18)	0.886	0.883 (4)	0.886 (8)
$\lambda_{\text{scint}} (\mu\text{s}^{-1})$	-	0.0132 (8)	-	0.00132
$\epsilon$ (%)	-	86.0 (3)	-	4 (9)

parameters are significantly increased. This can be understood by looking at the correlations (Table 7.5), which reach alarmingly high levels when an extra depolarisation in the scintillator is allowed. In the case of 127  $\mu\text{m}$ , the fit is harmed by including an extra depolarisation in the scintillator. The remaining spin glass sets were fit with an extra scintillator depolarisation term, with  $\lambda_{\text{scint}} = 0.0132 \mu\text{s}$  fixed. The fit to Set A (target of SG only) would not succeed. For sets E (SG+Al) and H (Sg+Ag), the fractions of muons stopping in the scintillator were  $\epsilon = (0 \pm 10)\%$  and  $\epsilon = (8 \pm 8)\%$  respectively. The 127  $\mu\text{m}$  result in Table 7.4 found  $\epsilon = (4 \pm 9)\%$ . For all fits with two exponentials, the global correlations were worryingly close to 1.0. The effect on  $\lambda_{\text{SG}}$ ,  $A_b$  and  $A_f$  is shown in Fig. 7.4, where the statistical precision is worse, but the values do not systematically change.

Table 7.5: Global parameter correlations compared for fits with a single exponential and sum of exponentials, where the latter allows for separate depolarisation in the spin glass and scintillator.

Set Fit	Set I: SG+Ag, 508 $\mu\text{m}$ scint.		Set J: SG+Ag, 127 $\mu\text{m}$ scint.	
	Single $\lambda$	Converged	Single $\lambda$	Converged
$r$	0.983	0.997	0.956	1.000
$A_b$	0.880	0.994	0.802	1.000
$A_f$	0.878	0.995	0.745	1.000
$\lambda_{\text{SG}}(\mu\text{s}^{-1})$	0.952	-	0.907	-
$\lambda_{\text{scint}}(\mu\text{s}^{-1})$	-	0.951	-	0.979
$\epsilon$ (%)	-	0.972	-	1.000


 Figure 7.4: Effect on  $\lambda_{\text{SG}}$ ,  $A_b$  and  $A_f$  when a second exponential scintillator depolarisation with  $\lambda_{\text{scint}} = 0.0132 \mu\text{s}$  is included.

In another approach, a simultaneous fit was made to all sets, with  $\lambda_{\text{SG}}$  and  $\lambda_{\text{scint}}$  as common parameters. The minimiser was able to converge on a solution, but the uncertainties on the fit parameters could not be reliably determined. The global correlations were also close to 1.0. The relaxation rates were

$$\lambda_{\text{SG}} = (0.887 \pm 0.002) \mu\text{s}^{-1}, \quad (7.10)$$

$$\lambda_{\text{scint}} = (0.0123 \pm 0.0007) \mu\text{s}^{-1}, \quad (7.11)$$

which are consistent with the earlier approach. This approach also determined the fraction of scintillator stops for the nominal case as somewhere between 0 and 10%.

### 7.5.3 Metal samples

Fits were carried out on the metal foils, initially assuming 100% of muons stopped in the sample. The values of  $A_b$  and  $A_f$  were fixed to 0.185 and  $-0.238$ ; the dependence of the metal relaxation rate on this assumption will be tested later.

The asymmetry for muons stopping in the silver mask was analysed on a run-by-run basis as a consistency check. The mask was expected to be  $> 99.99\%$  purity, rather than the  $> 99.999\%$  purity of the TWIST silver foil. Figure 7.1 shows this is upstream of the regular target, and should be unaffected by what happens downstream. The results are shown in Fig. 7.5. There is little to say about the confidence levels, except for set E it's concerning they are all  $\leq 10\%$ . The  $r$  parameters are more interesting, since there are clear systematic steps whenever the target or running conditions are altered. The relaxation rates,  $\lambda$ , demonstrate some problems; for example, one run from set A is several  $\sigma$  from the average, set D has a negative relaxation rate (but a reasonable fit quality), and there is suggestion that set G has a systematically smaller rate than set H. These results are interesting, but it's not clear how the silver mask results can be used to establish a systematic uncertainty on the results from the TWIST foils.

The average value of  $\lambda$  for the reference silver is

$$\lambda = (1.07 \pm 0.07) \text{ms}^{-1}. \quad (7.12)$$

This result is stated with the caveat that Fig. 7.5 suggests the  $\lambda$  values are not consistent between runs.

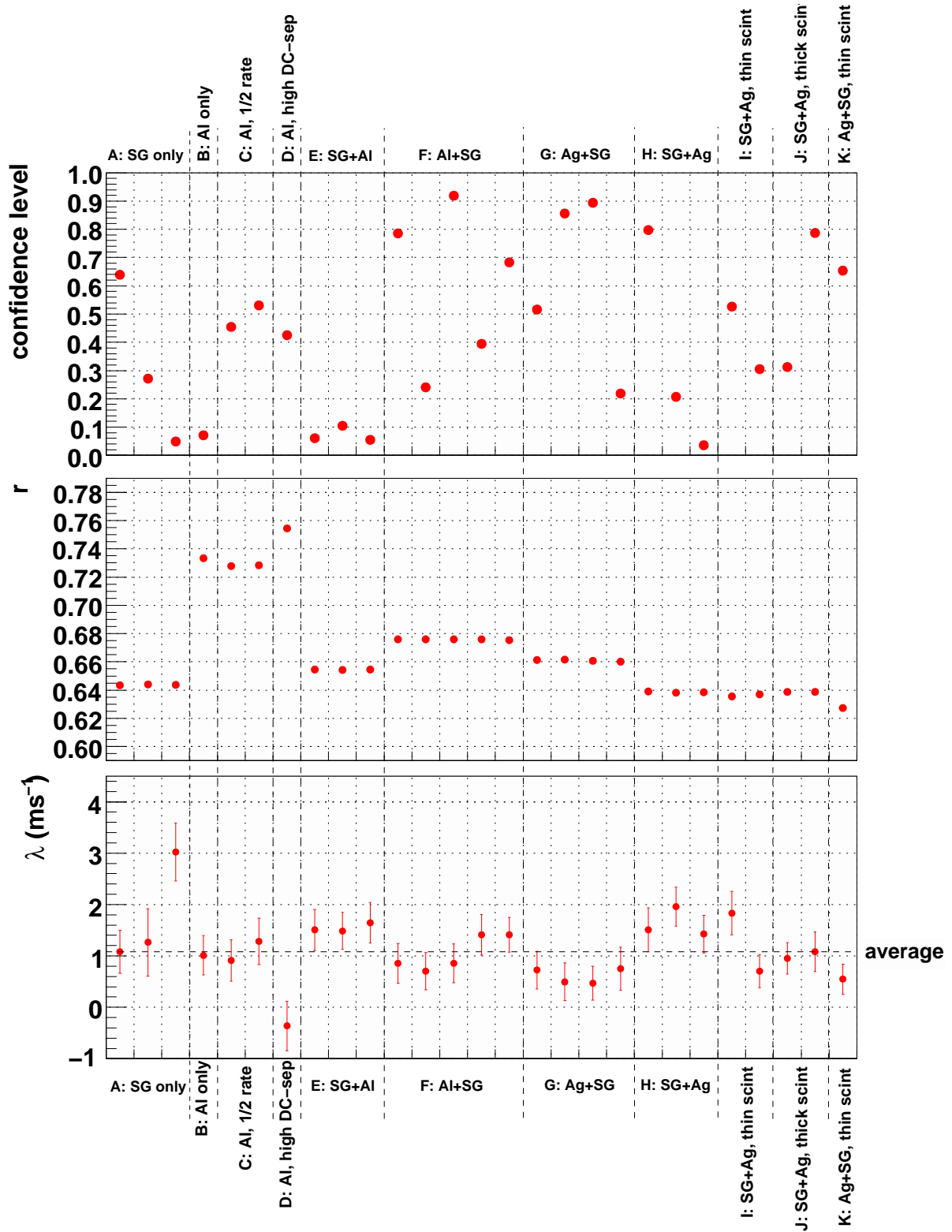


Figure 7.5: Important fit results for silver mask (99.99% purity). Each run was individually fit to monitor stability.

The results for the metal samples are shown in Table 7.6 and Fig. 7.6. Note that set C had two runs, but had to be summed to allow enough statistics for a fit. The confidence levels are reasonable except for the last run of set F. For this set, the relaxation rate is still consistent with the other runs, so it was not rejected. When the individual runs in sets F and G were summed, the confidence level of the fits were low (0.04 and 0.10 respectively). The  $r$  parameters show a similar pattern to the silver mask's values in Fig. 7.5. However, the relationship was not strong enough to impose a restraint. The relaxation rates for aluminium are consistent for sets B, C, D and F, with an average relaxation rate,

$$\lambda_{\text{Al}} = (1.7 \pm 0.2) \text{ms}^{-1}, \quad (7.13)$$

under the assumption that all muons stop in the target. Similarly, the relaxation rates for silver were consistent for sets G and K, yielding

$$\lambda_{\text{Ag}} = (1.2 \pm 0.2) \text{ms}^{-1}. \quad (7.14)$$

Table 7.6: Fit quality and parameters for the metal samples. The bracketed number indicates the uncertainty on the final digit.

Set	$\chi^2/\text{ndof}$	Confidence	$\lambda$ ( $\text{ms}^{-1}$ )	$r$
B: Al only	1.10	0.11	2.2 (5)	0.9000 (4)
C: Al, $\frac{1}{2}$ -rate	0.86	0.96	1.6 (3)	0.8981 (3)
D: Al, high DC-separator	1.04	0.29	1.3 (6)	0.9241 (6)
F: Al+SG	1.05	0.26	2.0 (5)	0.7402 (4)
	0.98	0.57	1.4 (5)	0.7399 (4)
	0.92	0.83	1.5 (5)	0.7400 (4)
	1.09	0.15	2.0 (5)	0.7403 (4)
	1.23	0.00	1.7 (4)	0.7403 (3)
G: Ag+SG	0.99	0.55	1.5 (5)	0.7062 (4)
	0.88	0.94	0.7 (5)	0.7069 (4)
	0.96	0.68	1.6 (4)	0.7057 (3)
	1.07	0.18	0.9 (5)	0.7067 (4)
K: Ag+SG, thin scint.	1.01	0.42	1.2 (4)	0.6603 (3)

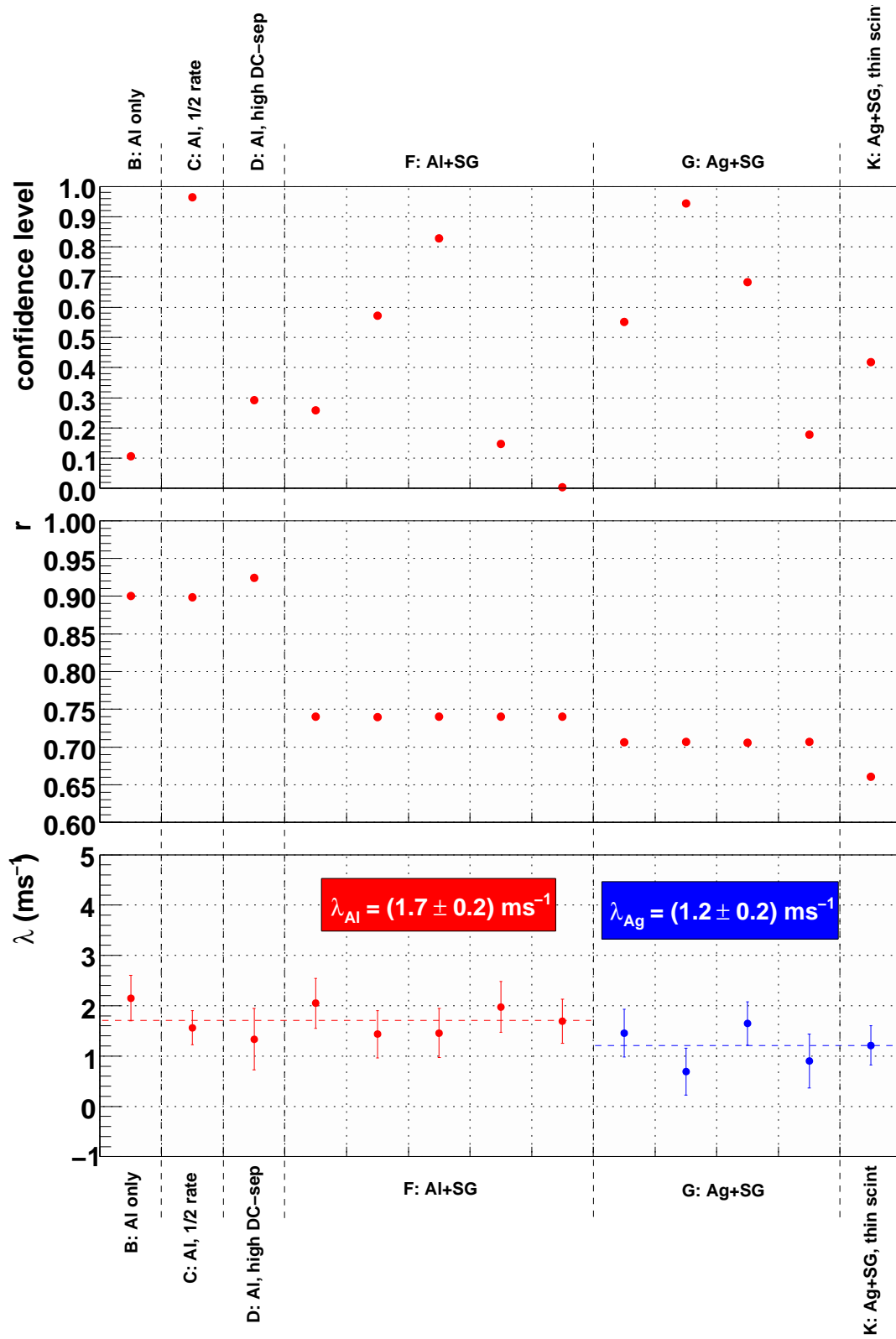
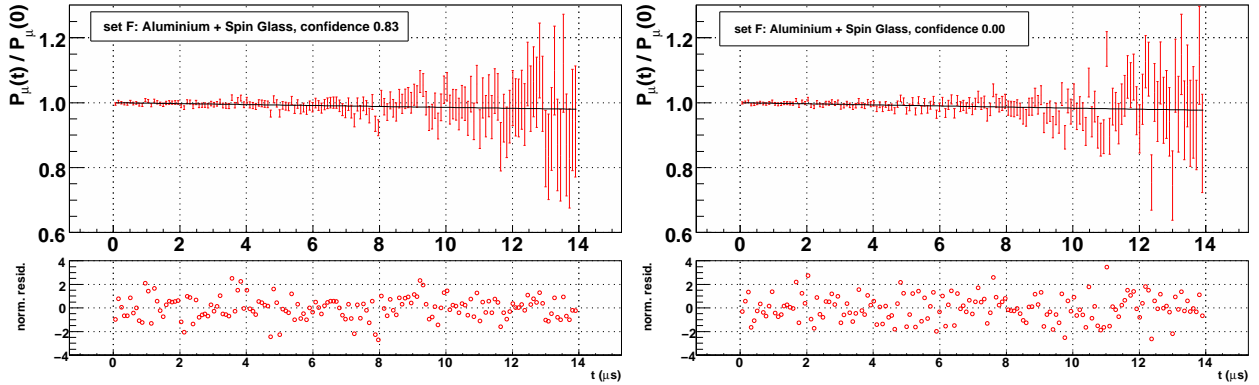


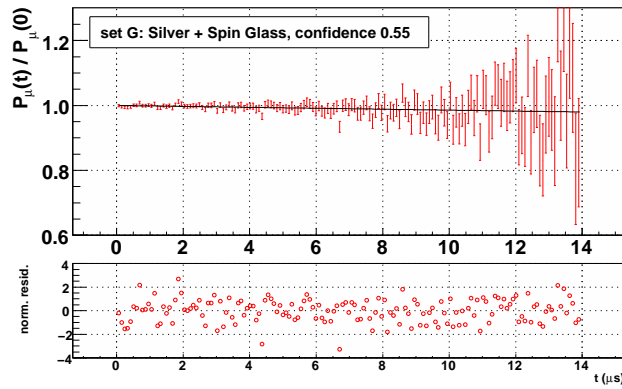
Figure 7.6: Important fit results for metal samples.

Figure 7.7 has the fit results for three runs, which show no evidence that anything beyond a single exponential is needed to describe the depolarisation. In Fig. 7.7(b), where the confidence level is low, there is a suggestion the binning may be imperfect. Note that fits were *not* made to the asymmetry; instead Eqs. 7.5 and 7.6 were used to fit the backward and forward histograms. In fact, the asymmetry figures cannot be constructed unless a model is assumed for  $P_\mu(t)$ .



(a) High confidence level, aluminium target.

(b) Low confidence level, aluminium target.



(c) Sample silver target result.

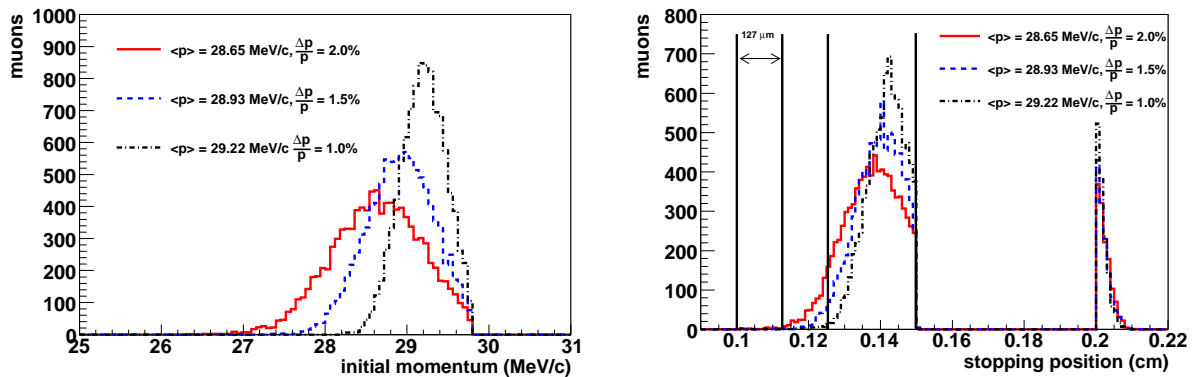
Figure 7.7: Example metal asymmetry fits and their normalised residuals.

## 7.6 Correction: scintillator stops

Section 7.5.2 found that somewhere between 0% and 10% of muons stop in the nominal scintillator. This is a problem, since the depolarisation rate in the scintillator is a factor  $\approx 10$  larger than the metal, allowing the possibility that all the depolarisation observed in the metal samples is actually due to depolarisation in the scintillator.

Since the data could not determine the fraction stopping in the scintillator with precision, a simulation was carried out[35]. The aim was to either obtain an absolute value for the fraction of stops in each scintillator, or a ratio between the thin and nominal scintillators. Software from the SRIM (the **S**topping and **R**ange of **I**ons in **M**atter) group of programs[55] was used, which includes full quantum mechanical treatment of ion-atom collisions[56] (in this case the “ion” was the muon).

The simulation required the initial momentum to be specified, but this was not measured during the data acquisition period. The M20 channel was set to maximise surface muon intensity, suggesting a minimal part of the momentum distribution lay beyond the kinematic cutoff at 29.79 MeV/c. Therefore simulations were run with conservative estimates of the RMS, and the central momentum adjusted to be  $2\sigma$  below the kinematic cutoff. The initial momentum distributions are shown in Fig. 7.8(a).



(a) Initial momentum used in the simulations.

(b) Stopping distributions for the different initial momentums.

Figure 7.8: Initial momentum distributions used in the SRIM simulation, and the resulting stopping distributions.

In each simulation, the thickness of a piece of Mylar was adjusted to make 13% of muons stop in the metal target. Instead of running separate simulations for each scintillator, a single

simulation was run for each momentum but with three pieces of scintillator in place:  $127\ \mu\text{m}$ ,  $127\ \mu\text{m}$  and  $254\ \mu\text{m}$ . This allowed the fraction of stops in three thicknesses of scintillator ( $127\ \mu\text{m}$ ,  $254\ \mu\text{m}$  and  $508\ \mu\text{m}$ ) to be determined simultaneously by integrating the number of stops appropriately. The stopping distributions are shown in Fig. 7.8(b), and the relevant numbers are in Table 7.7.

Clearly the initial momentum distribution is important in such a simulation, and it was a mistake to not make a measurement while acquiring data. The table of results show it is possible to obtain anything from 0.5% to 5.9% muon stops in the nominal scintillator, which disfavours the data's suggestion of up to 9%. The simulation shows it's hard to find more than 0.2% of muons stopping in the thin scintillator.

Table 7.7: The table shows the fraction of muons that would stop in each scintillator for each initial momentum choice.

$\langle p \rangle$ (MeV/c)	$\Delta p/p$ (RMS)	Fraction of stops (%)		
		thin ( $127\ \mu\text{m}$ )	nominal ( $254\ \mu\text{m}$ )	thick ( $508\ \mu\text{m}$ )
29.22	0.010	$0.07 \pm 0.03$	$0.5 \pm 0.1$	$85.8 \pm 0.9$
28.93	0.015	$0.09 \pm 0.03$	$1.9 \pm 0.1$	$86.8 \pm 0.9$
28.65	0.020	$0.22 \pm 0.05$	$5.9 \pm 0.2$	$86.7 \pm 0.9$

A systematic uncertainty can be estimated by re-fitting the metal with a fraction of muons forced to depolarise in the scintillator. Figure 7.9 shows the result for between 0% and 10% scintillator stops. If the central value of  $\lambda$  is corrected so that  $\epsilon = 3.5\%$ , with an uncertainty that allows for between 1% and 6% scintillator stops, then the nominal scintillator results are

$$\lambda_{\text{Al}} = (1.3 \pm 0.2 \text{ (stat.)} \pm 0.3 \text{ (syst.)}) \text{ ms}^{-1} \quad (7.15)$$

$$\lambda_{\text{Ag}} = (0.9 \pm 0.2 \text{ (stat.)} \pm 0.2 \text{ (syst.)}) \text{ ms}^{-1}. \quad (7.16)$$

For the single run with the thin ( $127\ \mu\text{m}$ ) scintillator, the contribution from scintillator stops is negligible, but the statistical uncertainty dominates so that

$$\lambda_{\text{Ag}} = (1.2 \pm 0.4) \text{ ms}^{-1}. \quad (7.17)$$

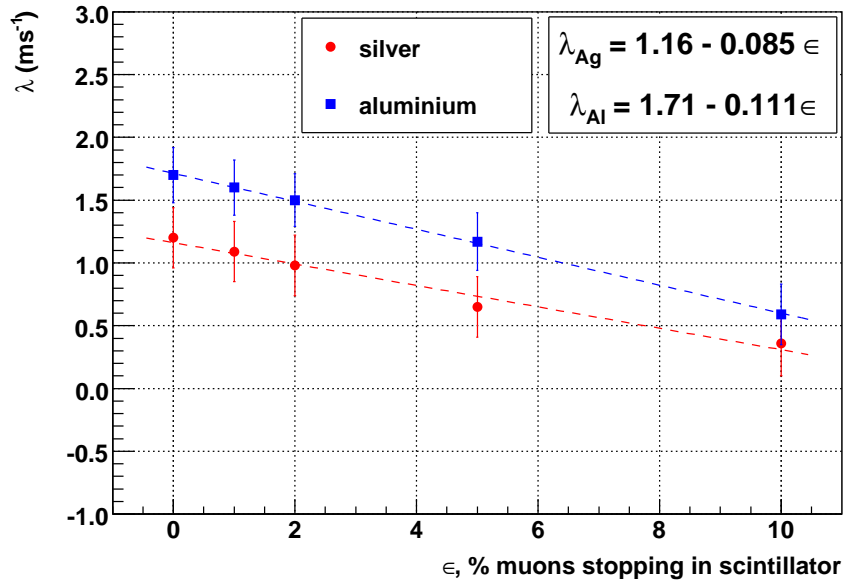


Figure 7.9: The exponential depolarisation for silver and aluminium, as muons are forced to stop and depolarise in the scintillator.

## 7.7 Other systematic uncertainties

There is a systematic uncertainty from the fixed  $A_b$  and  $A_f$  values that were used in the metal fits. A 10% change in either of these parameters altered the relaxation rate by at most  $0.12 \text{ ms}^{-1}$ .  $A_b$  and  $A_f$  are determined with statistical precision  $< 0.3\%$ , but were forced to be  $A_b = 0.185$  and  $-0.238$  for all fits, which meant they were wrong by up to 2% (see Table 7.3). An estimate of the systematic uncertainty on the relaxation rate is  $(2/10) \times 0.12 = 0.02 \text{ ms}^{-1}$ . This is negligible compared to the systematic from the scintillator stops.

There was no systematic uncertainty assigned due to the background having a time structure. Figure 7.6 showed that confidence levels were reasonable, except for one set, which still produced a consistent relaxation rate. If the confidence levels were lower, or the relaxation rate for the low confidence level had been anomalous, a systematic uncertainty due to the time structure of the background might have been necessary<sup>48</sup>

Figure 7.6 showed there was no evidence of a relaxation rate dependence on muon rate or DC separator setting. Therefore no systematic uncertainties are assigned for these effects.

<sup>48</sup>If the background was the leading systematic uncertainty, then a further investigation could revisit the calculations presented in Appendix 3 of Ref. [57], where time dependences due to pile-up are discussed.

## 7.8 Conclusions

The most precise result from the  $\mu^+$ SR analysis were

$$\lambda_{Al} = (1.3 \pm 0.2 \text{ (stat.)} \pm 0.3 \text{ (syst.)}) \text{ ms}^{-1} \quad (7.18)$$

$$\lambda_{Ag} = (0.9 \pm 0.2 \text{ (stat.)} \pm 0.2 \text{ (syst.)}) \text{ ms}^{-1}. \quad (7.19)$$

Later these will be confirmed as consistent with the results from the TWIST detector. Unfortunately the statistical precision from  $\mu^+$ SR is equivalent to less than one set from the TWIST detector, and the  $\lambda$  result is therefore only useful as a consistency check. The dominant systematic uncertainty cannot be reduced without accumulating more data. The most important conclusion from  $\mu^+$ SR is that a single exponential is appropriate down to 10 ns, and there is no evidence of a “fast” depolarisation being missed in the TWIST analysis.

There are several recommendations to make for a future experimenter. The dominant systematic uncertainty could have been reduced by carrying out momentum calibrations (and then not adjusting the beam line), measuring the depolarisation for a pure scintillator stopping target, and accumulating nominal data using a thin (127  $\mu\text{m}$ ) trigger scintillator. The fit quality could have been improved by including a time dependence to the background, but this would only be appropriate if more statistics were acquired, which would take far more than two weeks of beam time at TRIUMF. We were unable to find a constraint using the reference silver mask fit parameters; for example, the  $r$  parameter from the silver mask and regular metal fits were highly correlated, and it may have been possible to constraint them. A detailed simulation would have allowed such constraints to be investigated.